PHYSICAL REVIEW B **79**, 180511(R) (2009)

Using sideband transitions for two-qubit operations in superconducting circuits

P. J. Leek,* S. Filipp, P. Maurer, M. Baur, R. Bianchetti, J. M. Fink, M. Göppl, L. Steffen, and A. Wallraff
Department of Physics, ETH Zurich, CH-8093 Zurich, Switzerland

(Received 16 December 2008; revised manuscript received 15 April 2009; published 29 May 2009)

We demonstrate the time-resolved driving of two-photon blue sideband transitions between superconducting qubits and a transmission line resonator. As an example of using these sideband transitions for a two-qubit operation, we implement a pulse sequence that first entangles one qubit with the resonator and subsequently distributes the entanglement between two qubits. We show the generation of 75% fidelity Bell states by this method. The full density matrix of the two-qubit system is extracted using joint measurement and quantum state tomography and shows close agreement with numerical simulation.

DOI: 10.1103/PhysRevB.79.180511 PACS number(s): 85.25.−j, 03.67.Lx, 03.67.Bg, 42.50.Pq

In the pursuit of a scalable architecture for quantum information processing, Josephson-junction-based superconducting circuits are currently a leading candidate.[1] Controlled coherent two-qubit interactions, essential for the realization of universal quantum computation, have been demonstrated using a variety of coupling schemes.[2–7] A promising recent advance in the field has been the realization of circuit quantum electrodynamics (QED) (Ref. 8) in which superconducting qubits are strongly coupled to single photons in a transmission line resonator. This architecture has been used to couple two qubits over a distance of several millimeters by an exchange of a virtual photon between two resonant transmon qubits detuned from the resonator[5] and by an exchange of a real photon between two phase qubits in resonance with the resonator.[6] The possibility to achieve such nonlocal couplings is advantageous for the realization of multiqubit systems. It is also desirable to be able to switch two-qubit couplings on and off with high accuracy, such that high fidelity operations can be carried out both on individual qubits, and on specifically chosen pairs of qubits, avoiding spurious couplings to other qubits in the system. This issue can be addressed in superconducting circuits by controlling the interaction strength between two qubits via an external parameter[7] or by tuning transitions into and out of resonance.[3,5,6]

In this Rapid Communication, we present an experimental realization of a two-qubit coupling scheme in circuit QED that uses sideband transitions between the joint qubit and resonator states, in a similar manner to that achieved in ion traps.[9] In this scheme, qubit transition frequencies can be kept at well-separated values, chosen for optimal coherence, and do not need to be tuned during operations. The detuning between qubits can be chosen large enough such that qubits are never directly coupled and interact with the resonator only during driving of the sidebands. These features make the scheme attractive for scaling up to larger systems.

In the dispersive regime of circuit QED, the qubit transition frequency ω_A is detuned from the resonator frequency ω_r by $\Delta=|\omega_r-\omega_A|\gg g$, where g is the coupling strength between resonator and qubit on resonance [see Fig. 1(a)]. Although the qubit and resonator do not directly exchange energy in this case, the residual dispersive coupling still allows sideband transitions linking the qubit and resonator states to be accessed using strong additional microwave drive fields. Blue sideband transitions involve simultaneous excitation of both qubit and resonator at a transition frequency $\omega_A^+=\omega_r+\omega_A$, while the red sideband involves the exchange of an excitation between the two systems at a transition frequency $\omega_A^-=|\omega_r-\omega_A|$. These transitions have been observed in previous experiments on superconducting circuits[10,11] and also studied theoretically in the context of their use for quantum computation.[12,13]

Due to symmetry considerations in the circuit QED Hamiltonian, single-photon sideband transitions with either a Cooper pair box (CPB) (Ref. 14) biased at charge degeneracy or a transmon qubit[15,16] are forbidden to first order. They may, however, be accessed using two photons, whose sum or difference frequency is equal to one of the sideband transition frequencies $\omega_A^{+/-}$.[12] In earlier work with a CPB,[11] these two-photon transitions were observed in spectroscopy by applying two microwave fields of different frequency detuned slightly from the qubit and resonator. The increased coupling strength of the transmon to the resonator[15] compared to the CPB allows driving of the sidebands at larger detunings of the drives from the qubit and resonator. Here we choose to drive the blue sideband with two photons of equal energy, using a single microwave drive of frequency $\omega_A^+/2=(\omega_r+\omega_A)/2$ [see Fig. 1(b)]. In this configuration, the drive is equally detuned from the qubit and resonator, maximizing the selectivity of the sideband transition with respect to the undesired off-resonant driving of the bare-qubit transition and off-resonant population of the resonator.

We work with a two-qubit circuit QED device, for which

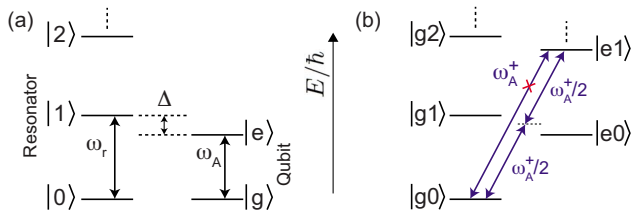

FIG. 1. (Color online) (a) Schematic of the energy levels of a harmonic oscillator with resonant frequency ω_r and levels $|n\rangle$ corresponding to photon number n and qubit with transition frequency ω_A and ground and first-excited states $|g\rangle$ and $|e\rangle$, respectively. (b) Combined level diagram, indicating the blue sideband transition $\omega_A^+=\omega_r+\omega_A$, which with one photon is forbidden to first order, but may be driven using two photons, for example, both at a frequency of $\omega_A^+/2$.

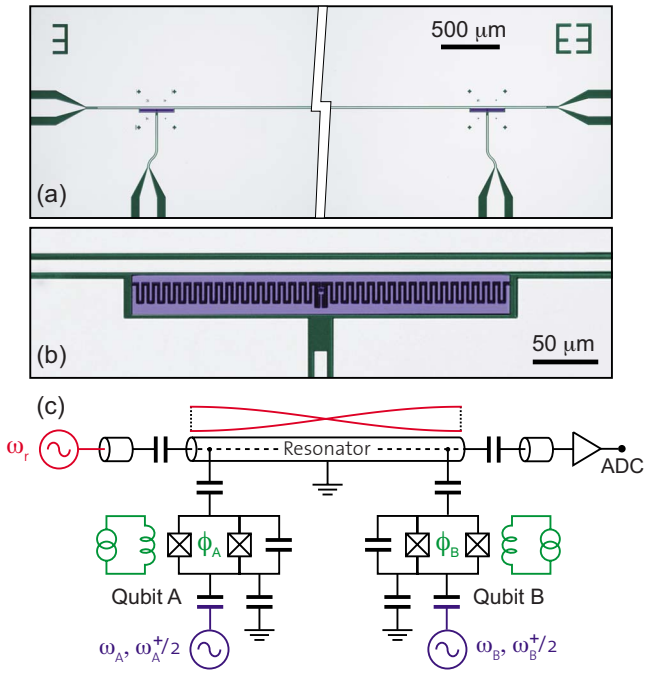

FIG. 2. (Color online) (a) False color optical microscope image of the two-qubit circuit QED device, with sapphire substrate in dark gray (green), niobium resonator in light gray (light blue), and aluminum qubits in medium gray (blue). (b) High magnification false color optical microscope image of one of the qubits coupled to the transmission line resonator and a local microwave drive line. (c) Electrical circuit representation of the two-qubit circuit QED device with local controls. The magnetic fluxes Φ_A and Φ_B through the SQUID loops of the qubits are tuned using local superconducting coils (green), while transitions are driven using local microwave drive lines (blue).

an optical image and circuit schematic are depicted in Fig. 2. A transmon qubit is fabricated at each end of a coplanar waveguide resonator with bare fundamental resonant frequency $\omega_r/2\pi=6.44$ GHz. The qubits labeled hereafter as qubits A and B are near identical, with a coupling strength to the resonator $g/2\pi=133$ MHz and a charging energy $E_C/h=232$ MHz. The transition frequencies of the qubits are tuned independently by changing the local magnetic fluxes Φ_A and Φ_B through the superconducting quantum interference device (SQUID) loops of qubits A and B, respectively, using two small superconducting coils mounted below the chip. Direct qubit and sideband transitions are driven selectively using microwave transmission lines coupled capacitively to each qubit locally [see Fig. 2(c)]. For the experiment, the qubits are tuned to transition frequencies of $\omega_A/2\pi=4.50$ GHz and $\omega_B/2\pi=4.85$ GHz, respectively, well into the dispersive regime.

Sweeping the frequency of a single strong microwave drive on one of the selective qubit drive lines and simultaneously measuring the resonator transmission to carry out a dispersive measurement of the qubit state[17] shows both the direct qubit transition at ω_A and an additional spectral line corresponding to the two-photon blue sideband at $\omega_A^+/2$ [see Fig. 3(a)]. The high selectivity of the individual qubit drive lines suppresses the coupling to qubit B, the transitions of

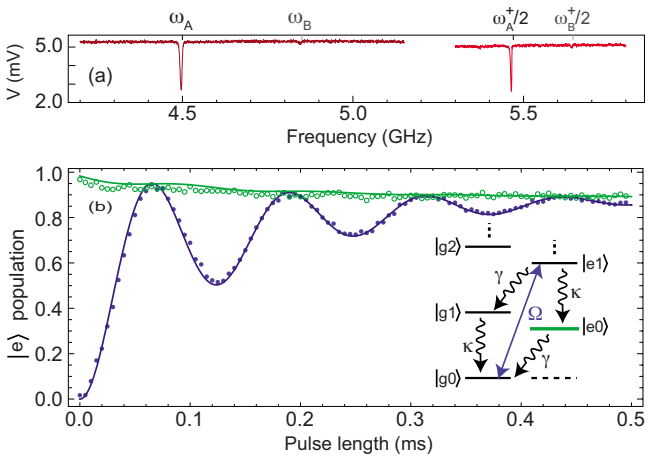

FIG. 3. (Color online) (a) Spectroscopy on the selective drive line of qubit A, showing the direct transition of the qubit at 4.50 GHz and the two-photon blue sideband at 5.47 GHz. (b) Time-resolved measurements of the excited-state population of qubit A as a function of the length of a blue sideband pulse. Blue solid circles show the response for the initial state $|g0\rangle$ and green open circles for $|e0\rangle$. Solid lines: master-equation simulations using decay parameters extracted from separate measurements. Blue and green again signify the initial states $|g0\rangle$ and $|e0\rangle$, respectively. (Inset) Level diagram showing competing drive and decay rates in the system.

which are barely visible in Fig. 3(a). The sideband spectral line is shifted to lower frequency at high drive amplitudes due to the ac-Stark effect on the bare-qubit transition.[18] At sufficient drive amplitude, time-resolved Rabi oscillations are observed on the blue sideband transitions [see Fig. 3(b)] by applying microwave pulses of fixed amplitude and varying length, at the Stark-shifted two-photon blue sideband frequency, to the local drive line of one qubit. The qubit excited-state population is then measured by applying a microwave pulse to the resonator and comparing the time evolution of the transmission to a numerical solution of the coupled qubit-resonator dynamics.[19]

Figure 3(b) shows the extracted excited-state population for such an experiment on qubit A (average of 6.6×10^4 repetitions). The solid blue data points show the results obtained when the system is initially in its ground state $|g0\rangle$, while green open data points correspond to an experiment in which the system is first excited to the state $|e0\rangle$ using a π pulse on the direct-qubit transition. In the latter case, no oscillations are observed since the state $|e0\rangle$ is not addressed by the blue sideband; a fact that was also observed in Ref. 10. Also shown in Fig. 3(b) (solid lines) are master-equation simulations of the evolution, using values for the qubit relaxation rate $\gamma/2\pi=0.2$ MHz and photon decay rate $\kappa/2\pi=1.7$ MHz taken from separate measurements, and with the blue sideband transition rate $\Omega/2\pi=8.15$ MHz as a fit parameter.

At long times it can be seen in Fig. 3(b) that the qubit excited-state population tends to a steady-state value of $p_{ss}\approx0.9$. This can be explained by considering the different drive and decay channels present in the system (see inset). Since the state $|e0\rangle$ has no blue sideband transition and

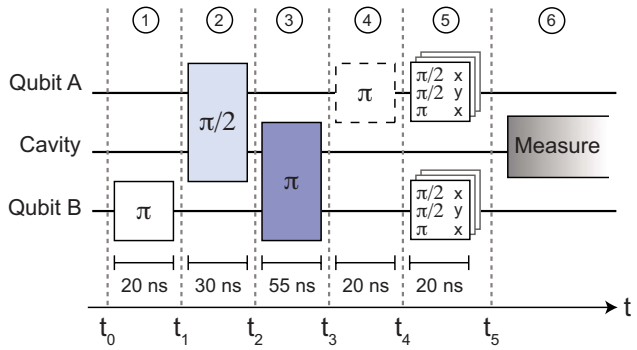

FIG. 4. (Color online) Pulse sequence implemented on the two-qubit and resonator system to generate and characterize qubit-qubit Bell states. Direct resonant qubit pulses are shown in white, while blue sideband pulses between resonator and qubits A and B are shown in light and dark blue, respectively. The ideal state of the system neglecting decay and imperfections after step i, at each of the intermediate times t_i is indicated in the text.

$\gamma \ll \kappa$, driving the sideband from the ground state $|g0\rangle$ results in a buildup of population in $|e0\rangle$. A simple model taking into account only the lowest four levels of the system predicts $p_{ss}=\kappa\Omega/(\kappa\Omega+\gamma\kappa+\gamma\Omega)=0.87$. It is worth noting that an increase in the ratio κ/γ would allow a high fidelity excited-state preparation by pumping of the blue sideband.

After characterizing the sideband Rabi oscillations for both qubits A and B, we proceed to demonstrate an example of a two-qubit operation based on the sidebands. We implement a pulse sequence designed to generate qubit-qubit entangled states (see Fig. 4), in a similar manner to that implemented in trapped ions.[20] At time t_0, the system is in its ground state $|gg0\rangle$, and a resonant π pulse is first applied to qubit B, generating the state $|ge0\rangle$ at t_1. A $\pi/2$ pulse on the blue sideband of qubit A then generates the entangled state $(|ge0\rangle+e^{i\phi'}|ee1\rangle)/\sqrt{2}$. The qubit-resonator entanglement is then transferred to qubit-qubit entanglement with a π pulse on the blue sideband of qubit B, generating the Bell state $|\Psi\rangle=(|ge\rangle+e^{i\phi}|eg\rangle)/\sqrt{2}$ at t_3, with the resonator returning to its ground state $|0\rangle$. The phase ϕ of the state is dependent on the phase difference between the two blue sideband pulses in the sequence. An additional resonant π pulse may now be applied to qubit A to generate the Bell state $|\Phi\rangle=(|gg\rangle+e^{-i\phi}|ee\rangle)/\sqrt{2}$ at t_4. The length of the full pulse sequence is $t_5-t_0\simeq 150$ ns, with the entanglement operation (pulses 2 and 3) lasting $t_3-t_1\simeq 90$ ns. During this time, the operation is sensitive to the photon lifetime $t_\kappa\simeq 95$ ns, which in the present sample is the limiting factor for the fidelity.

Full reconstruction of the two-qubit state may now be achieved using quantum state tomography. In contrast to previous approaches based on single-qubit single shot readout,[3] we employ an averaged joint two-qubit readout using the resonator transmission.[21] The preparation pulse sequence is repeated 16 times, with different combinations of additional final single qubit rotations (identity, $\pi/2_x$, $\pi/2_y$, and π_x on each qubit), and the resonator transmission is subsequently probed. The full density matrix is then parametrized in terms of the 16 averaged measurement results, and the closest physical density matrices are found using a maximum-likelihood approach.[22]

Examples of experimental two-qubit density matrices ρ measured after carrying out the pulse sequence for generation of the $|\Psi_+\rangle=(|ge\rangle+|eg\rangle)/\sqrt{2}$ and $|\Phi_+\rangle=(|gg\rangle+|ee\rangle)/\sqrt{2}$ Bell states are shown in Figs. 5(a) and 5(b). In each case 6.6×10^5 repetitions of the experiment were averaged. The fidelities $\mathcal{F}\equiv(\langle\psi|\rho|\psi\rangle)^{1/2}$ of the measured states ρ with respect to the perfect Bell states $\psi=\Psi_+$ and Φ_+ are $\mathcal{F}=74\%$ and 76%, respectively. We have repeated the state preparation 33 times and calculated the fidelities separately each time, obtaining an average fidelity of $75\pm 2\%$ for the full set. The entanglement of formation[23] of the generated states is 0.09 ± 0.04.

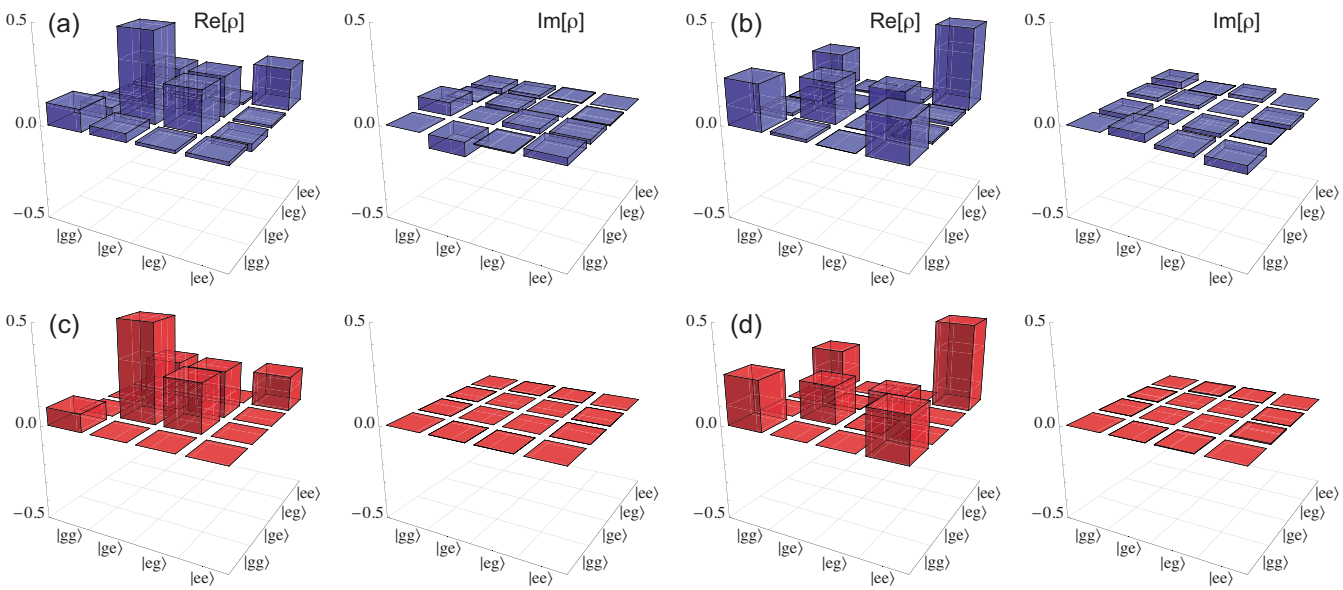

FIG. 5. (Color online) [(a) and (b)] Real and imaginary parts of the two-qubit density matrix extracted from two-qubit tomography measurements after carrying out the pulse sequence to generate the Bell states $|\Psi_+\rangle$ and $|\Phi_+\rangle$, respectively. [(c) and (d)] Simulated density matrices corresponding to the states shown in (a) and (b), respectively.

Also shown in Figs. 5(c) and 5(d) are density matrices resulting from a master-equation simulation, displaying very close agreement to the experimental matrices. The simulation makes both the dispersive and rotating wave approximations. Two energy levels for each qubit and the first five levels of the harmonic oscillator are taken into account. Energy relaxation and decoherence rates for the three individual systems are taken from separate measurements; the dominant loss contribution being the photon lifetime.

Higher fidelity entangled states are likely to be within reach by this method by utilizing the longer photon lifetime of a higher-quality factor resonator. The scheme may then be extendable to the implementation of a universal controlled NOT gate,[9,24] and should scale well to a system with a larger number of qubits. The sidebands may also be used to generate nonclassical states of the microwave field in the resonator such as Fock states.

We thank A. Blais, J. M. Gambetta and H. Häffner for valuable discussions and comments on the manuscript. We acknowledge the group of M. Siegel at the University of Karlsruhe for the preparation of Niobium films. This work was supported by ETH Zurich, the Swiss National Science Foundation, and by the EC via the EuroSQIP project and the Marie-Curie program (P. J. L.).

*leek@phys.ethz.ch

[1] J. Clarke and F. K. Wilhelm, Nature (London) **453**, 1031 (2008).
[2] T. Yamamoto, Y. A. Pashkin, O. Astafiev, Y. Nakamura, and J. S. Tsai, Nature (London) **425**, 941 (2003).
[3] M. Steffen, M. Ansmann, R. C. Bialczak, N. Katz, E. Lucero, R. McDermott, M. Neeley, E. M. Weig, A. N. Cleland, and J. M. Martinis, Science **313**, 1423 (2006).
[4] J. H. Plantenberg, P. C. de Groot, C. J. P. M. Harmans, and J. E. Mooij, Nature (London) **447**, 836 (2007).
[5] J. Majer, J. M. Chow, J. M. Gambetta, J. Koch, B. R. Johnson, J. A. Schreier, L. Frunzio, D. I. Schuster, A. A. Houck, A. Wallraff, A. Blais, M. H. Devoret, S. M. Girvin, and R. J. Schoelkopf, Nature (London) **449**, 443 (2007).
[6] M. A. Sillanpää, J. I. Park, and R. W. Simmonds, Nature (London) **449**, 438 (2007).
[7] T. Hime *et al.*, Science **314**, 1427 (2006); A. O. Niskanen *et al.*, *ibid.* **316**, 723 (2007); S. H. W. van der Ploeg, A. Izmalkov, A. M. van den Brink, U. Hubner, M. Grajcar, E. Ilichev, H. G. Meyer, and A. M. Zagoskin, Phys. Rev. Lett. **98**, 057004 (2007).
[8] A. Wallraff, D. I. Schuster, A. Blais, L. Frunzio, R.-S. Huang, J. Majer, S. Kumar, S. M. Girvin, and R. J. Schoelkopf, Nature (London) **431**, 162 (2004).
[9] F. Schmidt-Kaler, H. Häffner, M. Riebe, S. Gulde, G. Lancaster, T. Deuschle, C. Becher, C. Roos, J. Eschner, and R. Blatt, Nature (London) **422**, 408 (2003).
[10] I. Chiorescu, P. Bertet, K. Semba, Y. Nakamura, C. J. P. M. Harmans, and J. E. Mooij, Nature (London) **431**, 159 (2004).
[11] A. Wallraff, D. I. Schuster, A. Blais, J. M. Gambetta, J. Schreier, L. Frunzio, M. H. Devoret, S. M. Girvin, and R. J. Schoelkopf, Phys. Rev. Lett. **99**, 050501 (2007).
[12] A. Blais, J. M. Gambetta, A. Wallraff, D. I. Schuster, S. M. Girvin, M. H. Devoret, and R. J. Schoelkopf, Phys. Rev. A **75**, 032329 (2007).
[13] Y. X. Liu, L. F. Wei, J. R. Johansson, J. S. Tsai, and F. Nori, Phys. Rev. B **76**, 144518 (2007).
[14] V. Bouchiat, D. Vion, P. Joyez, D. Esteve, and M. H. Devoret, Phys. Scr. **T76**, 165 (1998).
[15] J. Koch, T. M. Yu, J. M. Gambetta, A. A. Houck, D. I. Schuster, J. Majer, A. Blais, M. H. Devoret, S. M. Girvin, and R. J. Schoelkopf, Phys. Rev. A **76**, 042319 (2007).
[16] J. A. Schreier, A. A. Houck, J. Koch, D. I. Schuster, B. R. Johnson, J. M. Chow, J. M. Gambetta, J. Majer, L. Frunzio, M. H. Devoret, S. M. Girvin, and R. J. Schoelkopf, Phys. Rev. B **77**, 180502(R) (2008).
[17] A. Wallraff, D. I. Schuster, A. Blais, L. Frunzio, J. Majer, M. H. Devoret, S. M. Girvin, and R. J. Schoelkopf, Phys. Rev. Lett. **95**, 060501 (2005).
[18] D. I. Schuster, A. Wallraff, A. Blais, L. Frunzio, R.-S. Huang, J. Majer, S. M. Girvin, and R. J. Schoelkopf, Phys. Rev. Lett. **94**, 123602 (2005).
[19] A. Blais, R. S. Huang, A. Wallraff, S. M. Girvin, and R. J. Schoelkopf, Phys. Rev. A **69**, 062320 (2004).
[20] C. F. Roos, G. P. T. Lancaster, M. Riebe, H. Häffner, W. Hänsel, S. Gulde, C. Becher, J. Eschner, F. Schmidt-Kaler, and R. Blatt, Phys. Rev. Lett. **92**, 220402 (2004).
[21] S. Filipp, P. Maurer, P. J. Leek, M. Baur, R. Bianchetti, J. M. Fink, M. Göppl, L. Steffen, J. M. Gambetta, A. Blais, and A. Wallraff, Phys. Rev. Lett. **102**, 200402 (2009).
[22] *Quantum State Estimation*, edited by M. G. A. Paris and J. Řeháček (Springer-Verlag, Berlin, 2004).
[23] C. H. Bennett, D. P. DiVincenzo, J. A. Smolin, and W. K. Wootters, Phys. Rev. A **54**, 3824 (1996).
[24] M. Riebe, K. Kim, P. Schindler, T. Monz, P. O. Schmidt, T. K. Körber, W. Hänsel, H. Häffner, C. F. Roos, and R. Blatt, Phys. Rev. Lett. **97**, 220407 (2006).